








The Novo Progresso Formation, Tapajós Gold Province, Amazonian Craton: zircon U-Pb and Lu-Hf constraints on the maximum depositional age, reconnaissance provenance study, and tectonic implications

Evandro Luiz Klein^{1*} , Stella Bijos Guimarães¹ , Joseneusa Brilhante Rodrigues¹ , Cesar Lisboa Chaves² , Sulsiene Machado de Souza Gaia² , Elem Cristina dos Santos Lopes², João Marcelo Rodrigues de Castro²

¹CPRM-Geological Survey of Brazil. SBN, Quadra 02, Bloco H, 1º andar, Brasília-DF, Brazil, CEP: 70040-904

²CPRM-Geological Survey of Brazil. Av. Dr. Freitas, 3645, Belém-PA, Brazil, CEP: 66095-110.

Abstract

The Novo Progresso Formation, located in southeastern Tapajós Gold Province, at its boundary with the Irixi-Xingu Domain, south of the Amazonian Craton, is composed of quartz- and lithic-arenites and siltstones with volcanic/volcanoclastic contributions, and was deposited in fluvial and lake systems. Reconnaissance detrital zircon U-Pb LA-ICP-MS data on a lithic arenite indicate maximum depositional age around 1840 Ma, whereas structural relationships suggest a minimum age of 1780 Ma. The zircon age spectrum shows two well-defined peaks at 1846 and 1968 Ma, and statistically secondary peaks ranging from 2185 Ma to 2973 Ma. ϵ_{Hf} values vary from +8.1 to -14.5 ($T_{\text{DM}} = 2.13$ to 3.95 Ga), whereas the ϵ_{Nd} values range from -2.5 to -3.3 ($T_{\text{DM}} = 2.31$ to 3.21 Ga), with one positive value of +4.5 ($T_{\text{DM}} = 1.81$ Ga). These data and the lithological composition indicate that surrounding Orosirian rocks from Tapajós and Irixi-Xingu were the main sources for the sediments, with subordinate contributions from older and more distant domains of the Amazonian Craton. In addition, the Hf systematics suggest a ~2.50 Ga-old crustal growth event and a ~3.95 Ga-old hidden component in the eastern portion of the Amazonian Craton. The deposition of the Novo Progresso Formation is related to the development of the large Orosirian intracratonic rift system known as Uatumã Silicic Large Igneous Province (1.89-1.80 Ga), which cut across the Amazonian Craton, following the final stages of magmatism in the Tapajós Gold Province.

Article Information

Publication type: Regular article
Submitted: 15 January 2018
Accepted: 13 April 2018
Online pub. 20 April 2018
Editor(s): JM Lafon

Keywords:

U-Pb, Hf isotopes,
Nd isotopes,
Paleoproterozoic,
Orosirian,
Sedimentology

*Corresponding author
Evandro Klein
E-mail address: evandro.klein@cprm.gov.br

1. Introduction

The sedimentary Novo Progresso Formation crops out in the southeastern portion of the Tapajós Gold Province, which evolved between about 2.05 and 1.76 Ga, central Amazonian Craton (Figs. 1 and 2). Santos (2003) and Ferreira et al. (2004) attributed an Orosirian age for this formation and related it to the development of a cratonic association (1.87 to 1.80 Ga) of the Irixi-Xingu Domain (east of the Tapajós Gold Province, Fig. 2), which includes the A-type granitoids of the Maloquinha Intrusive Suite and the still poorly understood Irixi Group (volcanic and pyroclastic rocks), both with ages ranging from 1.89 to 1.88 Ga. On the other hand, Vasquez et al. (2008), based on the spatial association of the Novo Progresso Formation with the volcanic and pyroclastic rocks of the Vila Riozinho Formation (Fig. 2), suggested a temporal relationship with this orogenic formation, which formed from 2001 to 1995 Ma (Lamarão et al. 2002) in the Tapajós Gold Province. Therefore, in addition to the controversial timing of sedimentation, the provenance of the sediments, and the tectonic setting of deposition remain unconstrained. In order to

address these issues, we make use of field and petrographic data, whole-rock Nd isotopes, along with the first U-Pb and Lu-Hf analysis of detrital zircon applied to the Novo Progresso sedimentary formation. As a result, we discuss the maximum depositional age, and present a reconnaissance investigation on the potential sources (provenance) for the zircon crystals contained in a lithic arenite of this formation.

2. Geology of the Tapajós Gold Province

The study area is located in the central portion of the Amazonian Craton, at the boundary zone between the Tapajós Domain (or Tapajós Gold Province – TGP, as used here) and the Irixi-Xingu Domain (Figs. 1 and 2). The TGP comprises a volcano-plutonic belt with subordinate metamorphic and sedimentary rocks (see the most recent compilation of the geology in the map of Vasquez et al. 2017b). The geological evolution of this domain spans from ca. 2050 Ma to ~1760 Ma. The metasedimentary Castelo dos Sonhos Formation was included in the TGP area by Klein et al. (2017). This formation is composed of auriferous

metaconglomerates and metasediments deposited by fan and fluvial systems between 2011 and 2050 Ma (Queiroz et al. 2015; Klein et al. 2017). The Cuiú-Cuiú Complex (2033 to 2005 Ma) is composed of amphibolite-facies orthogneisses and unmetamorphosed and undeformed coeval granitoids, which are partially associated with the greenschist facies metavolcano-sedimentary sequence of the Jacareacanga Group (~2010 Ma) (Santos et al. 2004; Vasquez et al. 2008). This association formed in a subduction-related setting (Tassinari and Macambira 2004; Santos et al. 2004; Vasquez et al. 2002, 2008). Undeformed and unmetamorphosed calc-alkaline felsic to intermediate volcanic and pyroclastic rocks occur in spatial and temporal association with the plutonic rocks and include the Comandante Arara (2020 to 2012 Ma) and Vila Riozinho (2002-1998 Ma) formations (Lamarão et al. 2005; Vasquez et al. 2017a). Batholiths of high-K, calc-alkaline granites of the Creporizão Suite intruded the Cuiú-Cuiú Complex between 1997 ± 5 and 1968 ± 7 Ma, and show geochemical characteristics of magmatic arc to post-collision rocks (Vasquez et al. 2002; Santos et al. 2004). The intrusion of the poorly-understood calc-alkaline tonalite to granite of the

Tropas Suite occurred between 1907 and 1892 Ma (Santos et al. 2001, 2004), slightly preceding the intrusion of voluminous batholiths and stocks of the Parauari Intrusive Suite of 1883-1879 Ma (Vasquez et al. 2008 and references therein). This suite comprises granodiorite and subordinate tonalite and other minor granitoid varieties that show high-K calc-alkaline signature (Vasquez et al. 2002, 2008). Both continental arc (Santos et al. 2004; Juliani et al. 2015) and post-orogenic extensional (Vasquez et al. 2002, 2008) settings have been invoked for the origin of this suite, which could be also related to the onset of the intracontinental rift system known as Uatumã Silicic Large Igneous Province (Uatumã SLIP – Klein et al. 2012). This rift was also filled by the alkaline granites of the Maloquinha Intrusive Suite and coeval alkaline volcanic and pyroclastic rocks of the Iriri Group (1895-1864 Ma; Lamarão et al. 2002; Santos et al. 2004; Vasquez et al. 2008), and by sedimentary rocks of the Novo Progresso Formation, as we will demonstrate below. This was followed by the establishment of Statherian sedimentary basins, such as the siliciclastic Crepori basin of up to 1780 Ma-old and the associated alkaline intracratonic magmatism (Fig. 2).

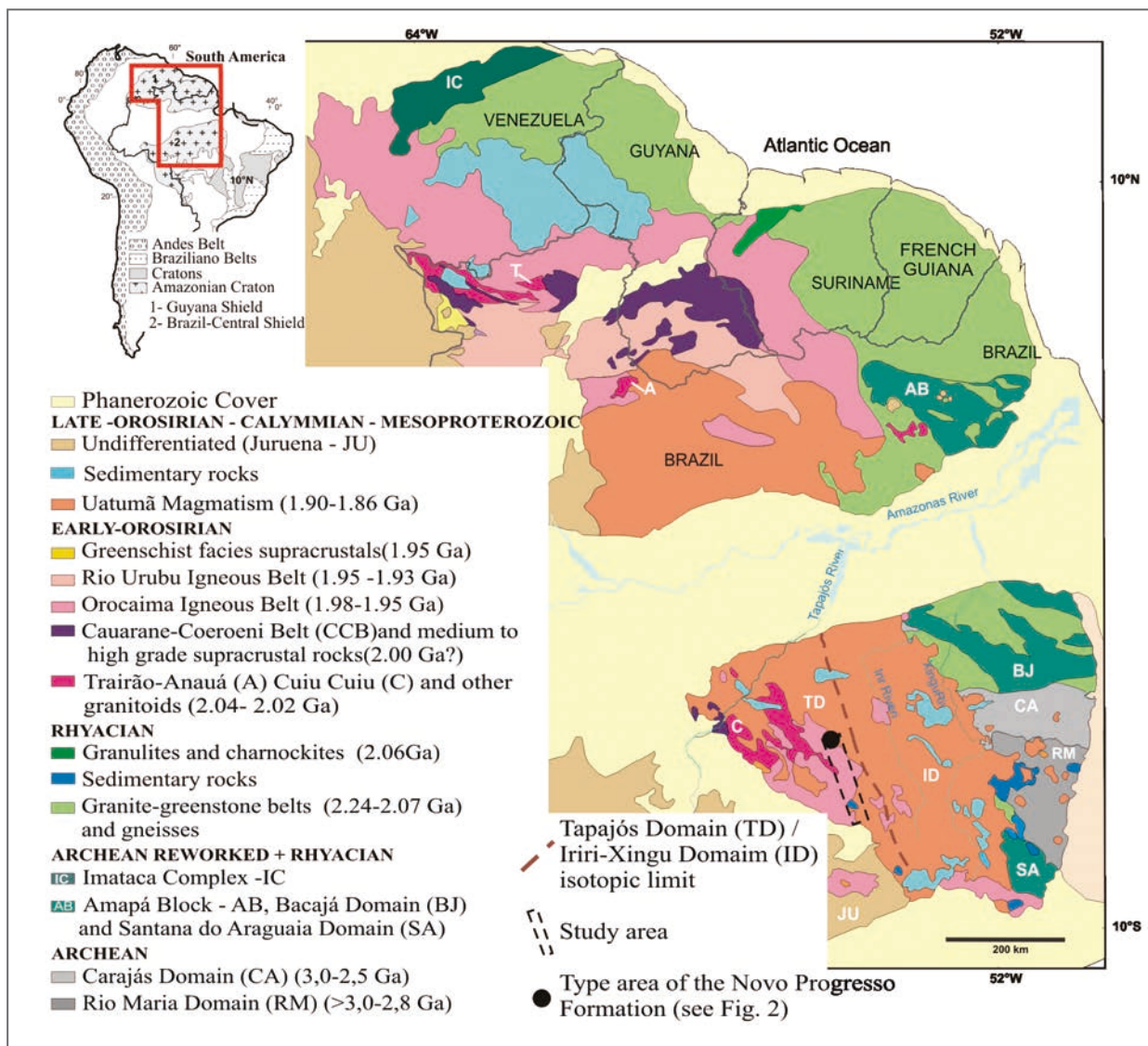


FIGURE 1 - Simplified geological map of the Amazonian Craton (modified from Fraga et al. 2017), with indications of the tectonic domains discussed in the text, and location of the study area.

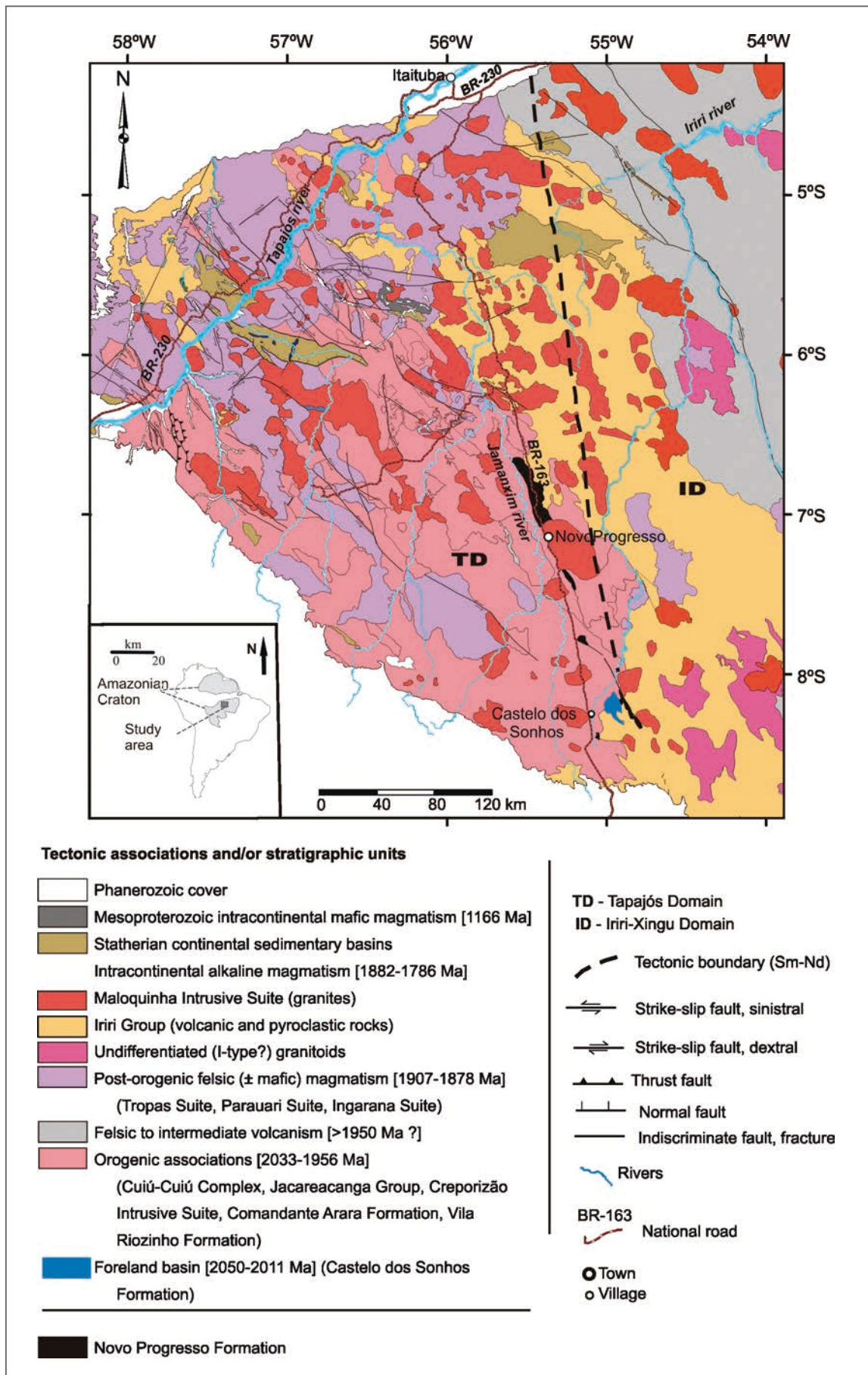


FIGURE 2 - Location (inset) and simplified map of tectonic associations of the Tapajós and Irixi-Xingu domains of the Amazonian Craton (modified from Vasquez et al. 2017).

The Iriri-Xingu Domain (Figs. 1 and 2) is broadly contained in the Uatumã-SLIP, in addition to calc-alkaline granitoids, felsic to intermediate volcanic rocks, and undifferentiated A- and I-type granitoids, with ages and petrographic characteristics similar to those found in the Creporizão, Parauari, Maloquinha and Vila Riozinho units of the TGP (Vasquez et al. 2008; Semblano et al. 2016). These magmatic rocks are covered by continental sedimentary rocks (Vasquez et al. 2008).

3. Summary of the geology and petrography of the Novo Progresso Formation

The Novo Progresso Formation crops out mostly as narrow NNW-SSE-trending low hills, which are parallel to the main regional structures, and five cropping areas have been recognized in southeastern TGP (Fig. 2). The formation is surrounded by granites of the Maloquinha, Parauari and Creporizão intrusive suites, felsic metavolcanic and pyroclastic rocks of the Vila Riozinho Formation and Iriri Group, and by metasedimentary rocks of the Castelo dos Sonhos Formation (Fig. 2). Contacts with these units are probably faulted and erosive. The rocks show sedimentary structures (stratification and lamination) that strike predominantly to N15-55°W/3-45°NE, which is grossly parallel to the regional structures, and locally to N50-70°E/75-84°NE (fault-related?). Cross-stratification occurs locally at N25°E/24°SE. This regional structural set differs from that of the Crepori sedimentary basin, which is grossly oriented to the E-W direction (Fig. 2), and associated to a younger Statherian (<1780 Ma) extensional event (e.g., Klein et al., 2017; Vasquez et al., 2017a). Therefore, a minimum depositional age of 1780 Ma is inferred for the Novo Progresso Formation.

In previous works, the Novo Progresso Formation has been described as composed of lower polymictic conglomerate with rounded to angular pebbles of granite, volcanic and volcanoclastic rocks, set in an arkosic matrix, and upper lithic sandstones and massive to layered, fine- to medium-grained arkose with intercalation of laminated argillite and siltstone (Ferreira et al. 2004; Vasquez et al. 2008). During field work we have found one conglomerate outcrop, that grossly fits with the described above, only outside the outcropping areas of the Novo Progresso Formation. Furthermore, our petrographic work has not identified arkosic rocks among the sandstones (see below).

The lithology, as observed in this work (Fig. 3), comprises: (1) massive to layered sandstone with plane-parallel and cross stratification and channeled sets (Fig. 4A to 4D) showing well-sorted, angular to subrounded quartz and feldspar grains, and lithic fragments, (2) relatively thick packages of purple to pinkish laminated siltstones (Fig. 4E), and (3) rhythmic intercalations of laminated siltstones and laminated, microcrystalline quartz-rich “cherty” rock (Fig. 4F), and of thin layers of massive argillite (Fig. 3).

Petrographically, the sandstones are lithic arenites and quartz arenites (Pettijohn 1975). The lithic arenites are composed of quartz (40-70%), feldspars (10-20%), lithic fragments (5-50%), opaque minerals (up to 2%), trace amounts of muscovite and zircon, and 7-20% of sericitized matrix (reworked ashes?). The rocks are well-sorted, with angular to subrounded grains. Quartz grains are mono to polycrystalline, but occur also as secondary overgrowth (cement) of detrital grains (Fig. 5A). Lithic fragments have major volcanic/tuffaceous contribution (predominantly felsic) and form elongated to subrounded fragments with impregnation of

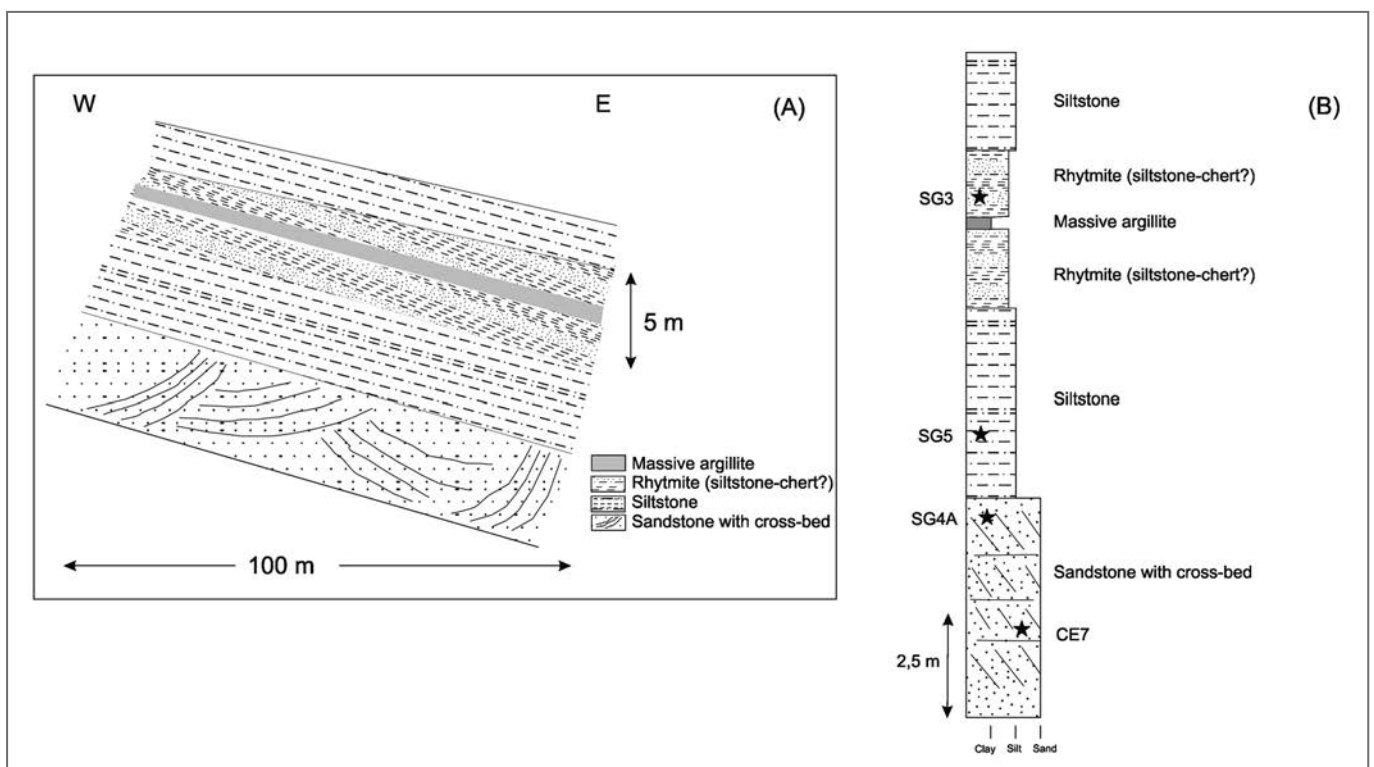


FIGURE 3. (A) Schematic W-E cross-section of the Novo Progresso Formation, and (B) interpreted sedimentary section, with the approximate location of samples used for isotopic analyses (black stars; sample numbers as in Table 4).

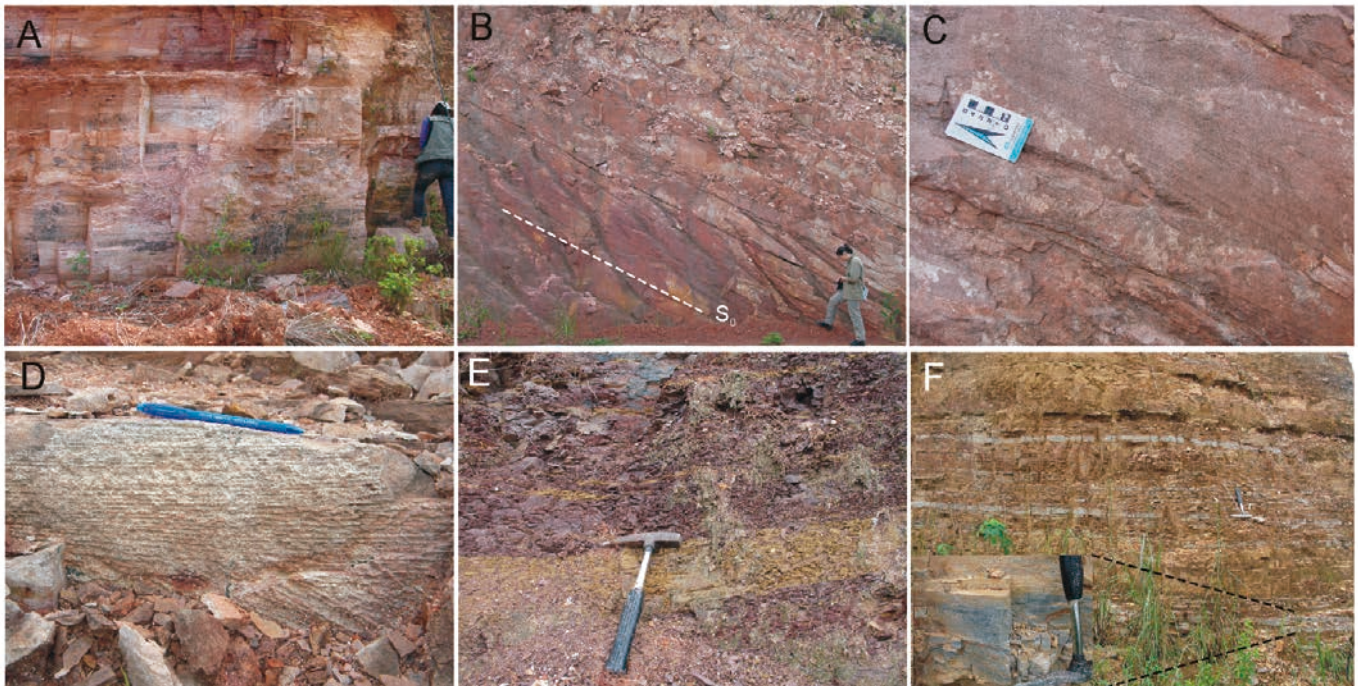


FIGURE 4 - Outcrop images of rock units of the Novo Progresso Formation. (A) Massive sandstone. (B) Sandstone with moderately dipping sedimentary bedding (S_0) and internal stratification. (C) Detail of sandstone with plane-parallel and cross stratification. (D) Channeled stratification in sandstone. (E) Laminated siltstones. (F) Package of brown siltstones with intercalation of light grey, fine grained quartz-rich (cherty) layers (detail in the inset).

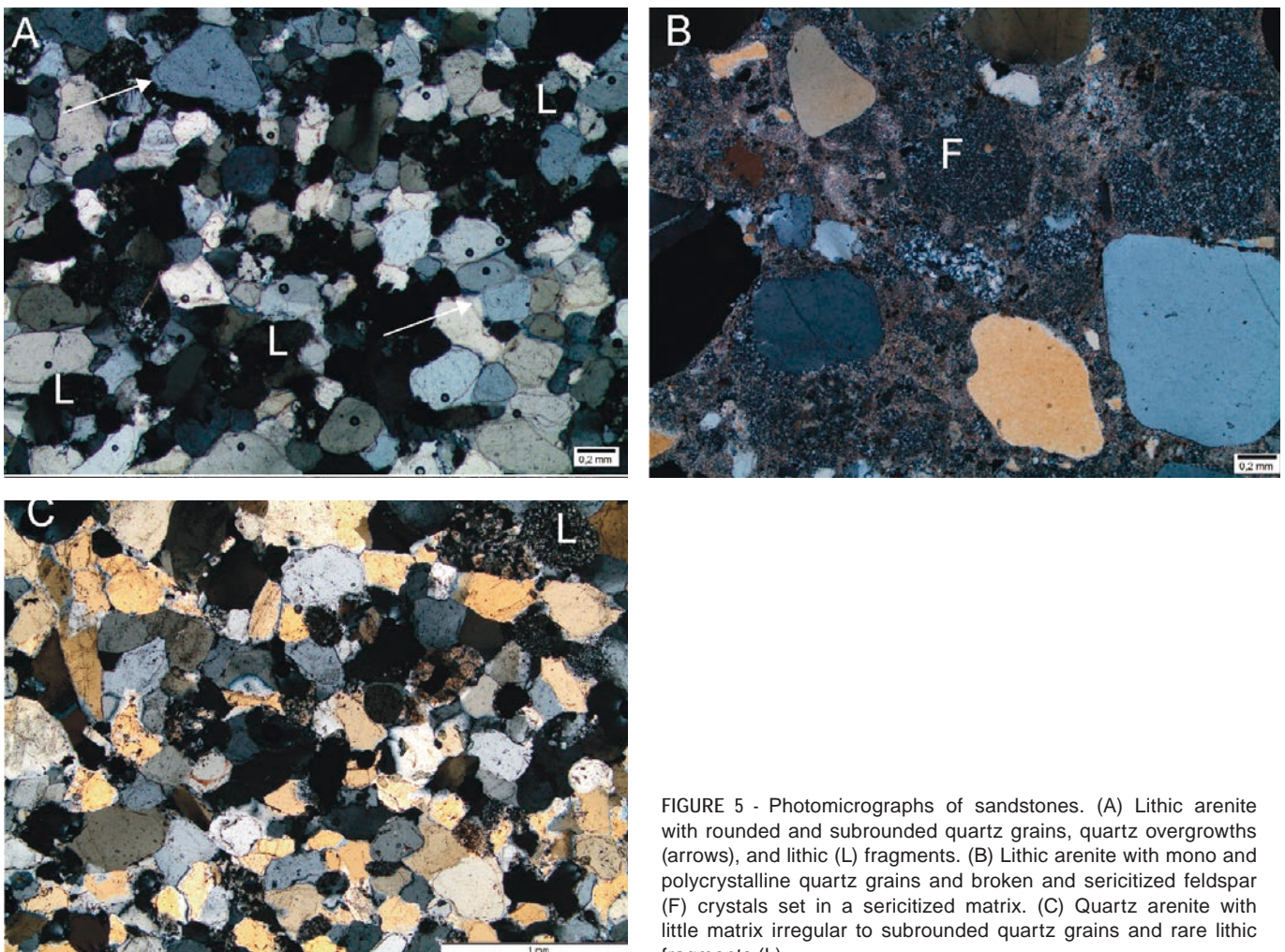


FIGURE 5 - Photomicrographs of sandstones. (A) Lithic arenite with rounded and subrounded quartz grains, quartz overgrowths (arrows), and lithic (L) fragments. (B) Lithic arenite with mono and polycrystalline quartz grains and broken and sericitized feldspar (F) crystals set in a sericitized matrix. (C) Quartz arenite with little matrix irregular to subrounded quartz grains and rare lithic fragments (L).

iron oxide/hydroxide. Feldspars occur as broken and altered (clay-sericite) fragments (Fig. 5B). The quartz arenites (Fig. 5C) have ~95% quartz, minor amounts of lithic fragments (1%), matrix (3-5%) and opaque minerals (<2%), along with trace amounts of feldspars, zircon and fluorite. Grains are well sorted and angular to subrounded, with irregularly-shaped lithic fragments.

4. Analytical procedures

Location of the samples analyzed in this study is listed in Table 1. In situ zircon U-Pb and Lu-Hf LA-ICP-MS analyses were undertaken at the Laboratório de Estudos Geocronológicos, Geodinâmicos e Ambientais of the Universidade de Brasília (UnB), Brasília, Brazil. The analyses followed procedures described in detail in Bühn et al. (2009) and Matteini et al. (2010) for the U-Pb and Lu-Hf techniques, respectively. Concentrates of zircon were obtained by crushing the rock and then sieving and panning. Zircon crystals with sizes between 0.177 mm (80#) and 0.074 mm (200#) were hand-picked under a binocular microscope, mounted in epoxy resin, and polished with diamond paste. The analyses were performed with a Thermo Finnigan Neptune multicollector inductively coupled plasma mass spectrometer with an attached New Wave 213µm Nd-YAG solid state laser. For the U-Pb analysis, the acquisition followed a standard – sample bracketing technique with four sample analyses between a blank and a GJ-1 zircon standard. The accuracy was controlled using the zircon standard 91500. Ablation time and spot diameters were, respectively, 40 s and 30 mm for the U-Pb analyses, and 50 s and 40 mm for the Lu-Hf analyses. Raw data were reduced using an in-house program and corrections were done for background, instrumental mass-bias drift and common Pb, as described in Bühn et al. (2009). The ages were calculated using ISOPLOT 3.0 (Ludwig 2003) with 1σ uncertainties, and data presentation follows Gehrels (2012). Analyses were preceded by backscattered electron (BSE) imagery also done at UnB using a Scanning Electron Microscope FEI Quanta 450.

The Lu-Hf isotopic data were collected during ablation time of 50 s and using a spot size diameter of 40 mm. The signals of the interference-free ¹⁷¹Yb, ¹⁷³Yb and ¹⁷⁵Lu isotopes were monitored in order to correct for isobaric interferences of the ¹⁷⁶Yb and ¹⁷⁶Lu on the ¹⁷⁶Hf signal. The contribution of ¹⁷⁶Yb and ¹⁷⁶Lu were calculated using the isotopic abundance of Lu and Hf proposed by Chu et al. (2002). The contemporaneous measurements of ¹⁷¹Yb, ¹⁷³Yb permit to correct the mass-bias of Yb using the ¹⁷³Yb/¹⁷¹Yb normalization factor of 1.132685 (Chu et al. 2002). The Hf isotope ratios are normalized to ¹⁷⁹Hf/¹⁷⁷Hf value of 0.7325 (Patchett 1983). To calculate eHf(t) values, we have adopted the ¹⁷⁶Lu decay constant of 1.867x10⁻¹¹/year (Söderlund et al. 2004), the chondritic values of ¹⁷⁶Hf/¹⁷⁷Hf = 0.0336 and ¹⁷⁶Lu/¹⁷⁷Hf = 0.282785 (Bouvier et al. 2008), and the model depleted mantle with present day ¹⁷⁶Hf/¹⁷⁷Hf = 0.28325 and ¹⁷⁶Lu/¹⁷⁷Hf = 0.0388 (Griffin et al. 2000; updated by Andersen et al. 2009).

Whole-rock Sm-Nd analyses were also undertaken at the UnB laboratory and the analytical procedures are described in Gioia and Pimentel (2000). Fifty mg of whole-rock powders were mixed with a ¹⁴⁹Sm/¹⁵⁰Nd spike and dissolved in Savillex vessels. The Sm-Nd separation used

cation exchange Teflon columns with Ln-Spec resin, then Sm and Nd were deposited in Re filaments and the isotopic ratios were determined on a Thermo Finnigan Triton thermal ionization mass spectrometer. The Nd data were normalized to a ¹⁴⁶Nd/¹⁴⁴Nd ratio of 0.7219 and uncertainties in the Sm/Nd and ¹⁴³Nd/¹⁴⁴Nd ratios were about 0.4% (1s) and 0.005% (1s), respectively, based on repeated analysis of the BHVO-1 and BCR-1 standards. The crustal residence ages were calculated using the values of DePaolo (1988) for the depleted mantle (TDM).

TABLE 1 - Location of the samples analyzed in this study

Sample	Lat	Long	Rock type	U-Pb	Lu-Hf	Sm-Nd
MR79	-8,37962	-55,04848	Lithic arenite			
MR116	-8,27186	-54,83471	Quartz arenite			
CE7	-6,95047	-55,45340	Lithic arenite	x	x	x
SG3	-7,02071	-55,41951	Cherty rock			x
SG4A	-7,02162	-55,42080	Lithic arenite			x
SG4B	-7,02162	-55,42080	Siltstone			
SG5	-7,05840	-55,40733	Siltstone			x
SG66	-7,41381	-55,22444	Quartz arenite			

5. U-Pb and Lu-Hf data by LA-ICP-MS in detrital zircon

5.1. U-Pb results

U-Pb isotopic results were obtained for one lithic arenite (CE7), sampled in the type area of the Novo Progresso Formation (43 crystals). Only the isotopic results of 37 grains with less than 10% discordance, analytical errors below 5%, and low common Pb concentrations (*f*₂₀₆ below 3%) are presented in Table 2 and were used for age and provenance interpretation.

Zircon crystals are mostly prismatic, with variable dimensions, rounded terminations, low to medium sphericity, oscillatory zoning, and show fractures and solid inclusions (Fig. 6A). In some crystals, irregular areas are observed around fractures, suggesting remobilization. Overgrowths were not identified. The ²⁰⁷Pb/²⁰⁶Pb apparent ages from 37 crystals range from 1835 ± 9 Ma to 2978 ± 11 Ma (Table 2). The age spectra show multimodal distribution (Fig. 6B), with two main peaks at 1846 and 1968 Ma. Important peaks occur at 2185 and 2505 Ma, and secondary peaks appear at 2065, 2109, 2327, 2365, 2686, 2842 and 2973 Ma. The youngest concordant crystal (0.7% discordance) yielded an age of 1836 ± 7 Ma.

5.2. Lu-Hf results

Lu-Hf isotopic results were obtained in 23 zircon crystals of the dated sandstone sample (CE7), and the analyses were performed on the same zircon domains that have previously been analyzed by the U-Pb technique. The selected zircons cover the detrital age populations and the analytical data are presented in Table 3.

TABLE 2 - U-Pb isotopic results for sample CE7 (lithic arenite) of the Novo Progresso Formation

Zircon	f206(%)	Th U	²⁰⁶ Pb ²⁰⁴ Pb	²⁰⁷ Pb ²⁰⁶ Pb	err (%) 1sigma	²⁰⁷ Pb ²³⁵ U	err (%) 1sigma	²⁰⁶ Pb ²³⁸ U	err (%) 1sigma	Rho	Apparent ages (1sigma)					Concordance %		
											²⁰⁷ Pb ²⁰⁶ Pb	(Ma)	²⁰⁷ Pb ²³⁵ U	(Ma)	²⁰⁶ Pb ²³⁸ U	(Ma)	6/8-7/6	6/8-7/5
Z01rim	0.43	0.26	3474	0.148907	0.68	8.263	1.96	0.402478	1.83	0.94	2333	12	2260	18	2180	34	93.4	96.4
Z01core	0.03	0.68	48897	0.152681	0.89	9.600	1.51	0.456036	1.22	0.80	2376	15	2397	14	2422	25	101.9	101.0
Z02	0.01	0.47	113180	0.121734	0.66	5.943	1.10	0.354048	0.87	0.78	1982	12	1967	9	1954	15	98.5	99.3
Z03	0.01	0.29	138005	0.121238	0.98	5.834	1.37	0.349026	0.95	0.81	1975	17	1952	12	1930	16	97.7	98.8
Z05	0.00	0.33	1080520	0.202542	0.65	14.416	1.12	0.516225	0.92	0.80	2847	11	2778	11	2683	20	94.2	96.6
Z06	0.00	0.43	405157	0.131293	0.71	6.877	1.02	0.379900	0.73	0.68	2115	12	2096	9	2076	13	98.1	99.0
Z07	0.02	0.72	99973	0.112467	1.27	4.723	1.82	0.304576	1.30	0.82	1840	23	1771	15	1714	19	93.1	96.7
Z08	0.01	0.47	303218	0.112971	0.87	4.859	1.29	0.311924	0.95	0.72	1848	16	1795	11	1750	15	94.7	97.4
Z09	0.01	0.54	227276	0.113767	0.85	4.946	1.28	0.315327	0.96	0.73	1860	15	1810	11	1767	15	94.9	97.6
Z10	0.03	1.30	43139	0.124206	3.16	6.642	3.59	0.387828	1.71	0.47	2018	55	2065	31	2113	31	104.7	102.3
Z11	0.01	0.39	137388	0.121661	1.05	5.787	1.52	0.344965	1.10	0.81	1981	19	1944	13	1911	18	96.4	98.2
Z12	0.01	0.59	187255	0.128121	0.70	6.199	1.20	0.350925	0.98	0.80	2072	12	2004	10	1939	16	93.5	96.7
Z13core	0.49	0.13	3155	0.121011	0.84	5.424	1.64	0.325062	1.40	0.85	1971	15	1889	14	1814	22	92.0	96.0
Z14	0.02	0.39	87640	0.121009	0.93	5.739	1.56	0.343949	1.25	0.79	1971	16	1937	13	1906	21	96.6	98.3
Z15	0.04	0.97	43190	0.115059	3.48	5.001	3.99	0.315264	1.96	0.73	1881	61	1820	33	1767	30	93.9	97.0
Z16	0.27	0.81	5450	0.138043	1.69	7.667	2.39	0.402812	1.68	0.70	2203	29	2193	21	2182	31	99.0	99.5
Z17	0.07	0.76	22653	0.132821	1.49	6.706	2.17	0.366171	1.57	0.72	2136	26	2073	19	2011	27	94.1	97.0
Z18	0.04	1.20	39022	0.185631	1.50	12.914	2.02	0.504568	1.36	0.83	2704	24	2673	19	2633	29	97.3	98.5
Z19	0.44	1.04	3553	0.114322	1.26	4.938	2.02	0.313268	1.57	0.77	1869	23	1809	17	1757	24	93.9	97.1
Z20	0.01	0.52	126839	0.138138	0.83	7.804	1.58	0.409740	1.34	0.84	2204	14	2209	14	2214	25	100.4	100.
Z21	0.01	0.42	129486	0.219621	0.69	17.352	1.83	0.573020	1.70	0.93	2978	11	2954	17	2920	40	98.0	98.8
Z22	0.01	0.34	152034	0.113481	1.21	5.315	1.72	0.339696	1.23	0.83	1856	22	1871	15	1885	20	101.5	100.7
Z23	0.38	0.50	4033	0.120965	0.77	5.748	2.06	0.344651	1.91	0.93	1971	14	1939	18	1909	32	96.8	98.4
Z24	0.01	0.57	110167	0.115428	0.99	5.737	1.85	0.360455	1.56	0.84	1887	18	1937	16	1984	27	105.1	102.4
Z25	0.01	0.44	147162	0.113349	0.60	5.225	1.30	0.334323	1.15	0.88	1854	11	1857	11	1859	19	100.3	100.1
Z26	0.03	0.58	53415	0.114404	1.42	5.114	1.97	0.324175	1.37	0.85	1871	25	1838	17	1810	22	96.7	98.4
NZ02	0.48	0.53	3307	0.112458	0.41	4.566	0.83	0.294480	0.72	0.85	1840	7	1743	7	1664	11	90.4	95.4
NZ03	0.01	0.40	226810	0.112170	0.52	5.599	0.90	0.362025	0.74	0.79	1835	9	1916	8	1992	13	108.5	103.9
NZ04	0.24	0.42	5893	0.165515	0.81	10.365	1.65	0.454174	1.44	0.87	2513	14	2468	15	2414	29	96.0	97.8
NZ07	0.00	0.65	295806	0.164943	0.37	11.436	1.02	0.502856	0.95	0.92	2507	6	2559	9	2626	20	104.7	102.6
NZ08	0.01	0.25	215442	0.114918	0.31	5.345	0.70	0.337344	0.63	0.87	1879	6	1876	6	1874	10	99.7	99.8
NZ09	0.00	0.17	967272	0.113194	0.36	5.769	0.81	0.369663	0.72	0.87	1851	7	1942	7	2028	12	109.5	104.4
NZ11	0.01	0.22	137139	0.119976	0.46	6.423	0.88	0.388261	0.75	0.83	1956	8	2035	8	2115	14	108.1	103.9
NZ13	0.01	0.55	155589	0.113288	0.57	5.353	1.04	0.342709	0.87	0.82	1853	10	1877	9	1900	14	102.5	101.1
NZ14	0.00	0.55	314354	0.112241	0.37	5.143	0.66	0.332310	0.54	0.77	1836	7	1843	6	1850	9	100.7	100.3
NZ15	0.05	0.21	32468	0.120885	0.48	5.771	1.04	0.346222	0.93	0.88	1969	8	1942	9	1917	15	97.3	98.6
NZ16	0.02	0.54	73754	0.136904	0.60	7.462	1.01	0.395324	0.81	0.78	2188	10	2168	9	2147	15	98.1	99.0

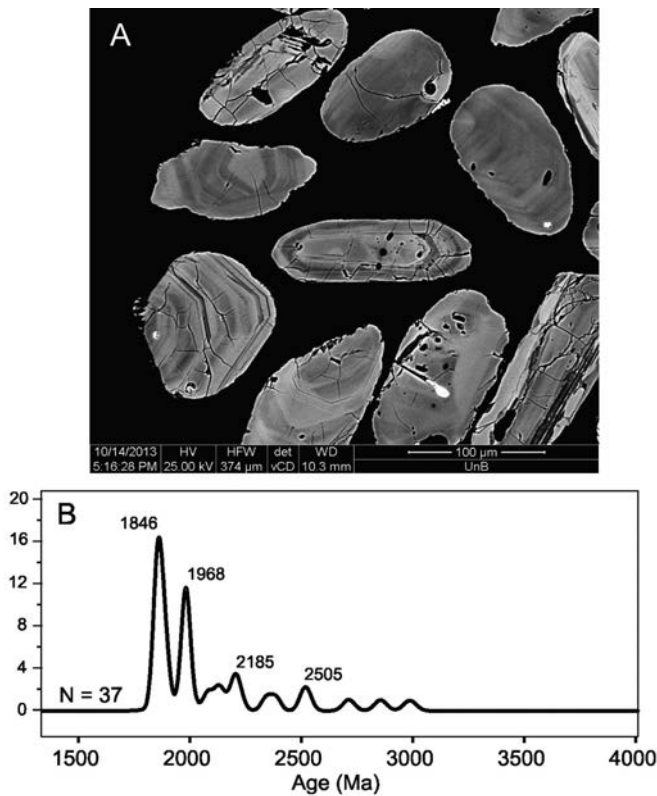


FIGURE 6 - (A) Backscattered electrons images of some detrital zircon images from sample CE7 (lithic arenite) of the Novo Progresso Formation. (B). Probability density plot of detrital zircon 207Pb/206Pb ages. The main age peaks are indicated.

There is no clear correlation between crystallization and depleted mantle model ages (TDM) (Fig. 7). Most of the model ages are in the range of 2.13 to 2.79 Ga, a few zircons show TDM between 2.95 and 3.12 Ga, and one zircon 3.95 Ga. The $\epsilon_{\text{Hf}}(t)$ values are highly variable, from +8.1 to -14.5 (one outlier at -44.9), and there is some difference between individual age populations. The two groups of Orosirian zircons (1.8 and 1.9 Ga) display almost the whole variation in the $\epsilon_{\text{Hf}}(t)$ values. The Rhyacian zircons show only slightly negative values, and the Archean zircons have highly positive to slightly negative values (Fig. 7). The highly positive value (zircon NZ04 in Table 3) indicates a 2.50 Ga-old event of crustal growth, whilst the model-age of 3.95 Ga (zircon Z15

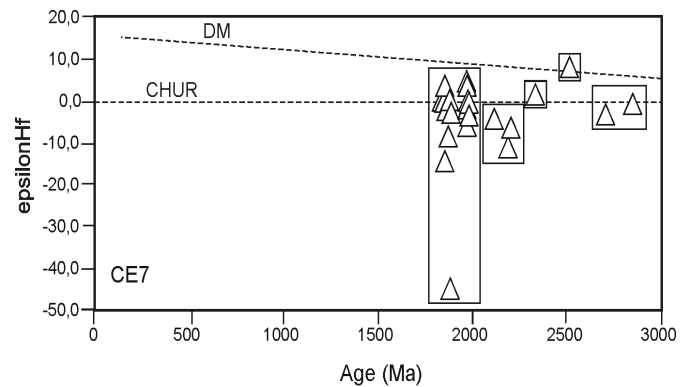


FIGURE 7 - Age versus epsilon ϵ_{Hf} plot for detrital zircon of the Novo Progresso Formation. DM = Depleted Mantle, CHUR = Chondritic Uniform Reservoir.

TABLE 3 - Detrital zircon LA-ICP-MS Lu-Hf results for sample CE7

Zircon/spot	Age (Ma)	$\pm 2\sigma$	$^{176}\text{Hf}/^{177}\text{Hf}$	$\pm 2\sigma$	$^{176}\text{Lu}/^{177}\text{Hf}$	$\pm 2\sigma$	$\epsilon_{\text{Hf}}(t)$	TDM (Ga)
Z01	2333	12	0.281380	0.000040	0.001083	0.000029	1.5	2.59
Z02	1982	12	0.281441	0.000043	0.000572	0.000006	-3.5	2.48
Z03	1975	17	0.281546	0.000030	0.000564	0.000007	0.1	2.34
Z05	2847	11	0.281007	0.000049	0.001435	0.000039	-0.8	3.12
Z06	2115	12	0.281349	0.000085	0.000963	0.000070	-4.3	2.63
Z08	1848	16	0.281642	0.000055	0.001239	0.000028	-0.3	2.25
Z09	1860	15	0.281565	0.000049	0.000850	0.000018	-2.2	2.33
Z11	1981	19	0.281536	0.000043	0.000772	0.000008	-0.4	2.36
Z13	1971	15	0.281667	0.000043	0.001114	0.000025	3.6	2.20
Z14	1971	16	0.281513	0.000070	0.001036	0.000034	-1.8	2.41
Z15	1881	61	0.280356	0.001445	0.001013	0.000027	-44.9	3.95
Z16	2203	29	0.281259	0.000845	0.001558	0.000022	-6.4	2.79
Z18	2704	24	0.280970	0.000043	0.000333	0.000013	-3.3	3.08
Z23	1971	14	0.281395	0.000045	0.000988	0.000013	-6.0	2.57
Z24	1887	18	0.281559	0.000147	0.001671	0.000021	-2.9	2.39
Z25	1854	11	0.281234	0.000036	0.001151	0.000015	-14.5	2.79
Z26	1871	25	0.281384	0.000048	0.000960	0.000009	-8.6	2.58
NZ04	2513	14	0.281452	0.000074	0.001133	0.000049	8.1	2.50
NZ08	1879	6	0.281656	0.000065	0.001848	0.000078	0.2	2.26
NZ13	1853	10	0.281865	0.000100	0.004633	0.000653	3.6	2.13
NZ14	1836	7	0.281681	0.000061	0.001948	0.000050	0.0	2.23
NZ15	1969	8	0.281697	0.000037	0.001031	0.000007	4.7	2.16
NZ16	2188	10	0.281120	0.000043	0.001144	0.000044	-11.1	2.95

in Table 3) suggests the existence of an Eoarchean hidden crustal component somewhere in the eastern part of the Amazonian craton.

6. Whole-rock Sm-Nd results

The whole-rock Sm-Nd concentrations and isotopic ratios, the calculated ϵNd values ($t = 1.85$ Ga) and the depleted mantle model ages (TDM) are shown in Table 4. The analyzed samples show low REE contents, with Sm ranging from 0.74 to 5.22 ppm, and Nd between 4.83 and 29.31 ppm. The Sm/Nd ratios and the fractionation factors [$f(\text{Sm-Nd})$] are within the normal range accepted for clastic sedimentary rocks (e.g., McLennan et al. 1993). The siltstone and one lithic arenite show model ages varying from 2.31 to 2.39 Ga, with $\epsilon\text{Nd}(t)$ values ranging from -2.5 to -3.2, whereas the laminated, microcrystalline “cherty” rock presents a model age of 1.81 Ga and $\epsilon\text{Nd}(t)$ value of +4.5. Another lithic arenite (CE7) shows an older model age, 3.12 Ga, and a value of -3.3 for $\epsilon\text{Nd}(t)$. This model age must be taken with caution, because the $^{147}\text{Sm}/^{144}\text{Nd}$ ratio is high (0.1663) and very close to the limit of 0.165 established by Stern (2002), above which the model becomes less reliable. This high $^{147}\text{Sm}/^{144}\text{Nd}$ ratio might have been produced by mafic contributions to the detritus (lithic fragments), although we cannot affirm this with confidence, given the fine-grained character of the lithic fragments.

TABLE 4 - Whole rock Sm-Nd data

Sample	Rock type	Sm (ppm)	Nd (ppm)	Sm/Nd	$f(\text{Sm/Nd})^*$	$^{147}\text{Sm}/^{144}\text{Nd}$	$^{143}\text{Nd}/^{144}\text{Nd}$	$\epsilon\text{Nd}(0)$	$\epsilon\text{Nd}(t=1.85\text{ Ga})$	$T_{\text{DM}}(\text{Ga})$
CE7	Lithic arenite	1.95	7.09	0.27511	-0.15455	0.1663	0.512099	-10.51	-3.3	3.12
SG4A	Lithic arenite	5.22	29.31	0.17825	-0.45196	0.1078	0.511392	-24.31	-3.2	2.39
SG3	Cherty rock	0.74	4.83	0.15404	-0.52669	0.0931	0.511608	-20.09	+4.5	1.81
SG5	Siltstone	4.45	26.46	0.16803	-0.48348	0.1016	0.511353	-25.07	-2.5	2.31

$$*f(\text{Sm/Nd}) = ^{147}\text{Sm}/^{144}\text{Nd}(\text{sample})/\text{CHUR} - 1$$

7. Discussions and conclusions

7.1. Provenance

Considering the limited amount of isotopic data produced in this study, we are aware that the discussion on provenance is of reconnaissance character, and that a larger dataset, in addition to sedimentological (e.g., paleocurrent) and quartz cathodoluminescence studies are necessary for a thorough provenance characterization. Despite this, our dataset allow that some reliable interpretations can be done. The two main age peaks of detrital zircon (1846 and 1968 Ma; Fig. 8A) indicate that surrounding Orosirian rocks from the Tapajós Gold Province and Irixi-Xingu Domain (including their counterparts in the Guyana Shield), and from the Rondonia-Juruena Province were probably the main sources for the sediments (Fig. 8A and 8B). This is consistent with the low maturity of the sediments and proximal sources. From the Hf and Nd isotopes results, the Orosirian rocks formed from variable contributions of Paleoproterozoic and Archean protoliths. Unfortunately, the lack of significant Hf data for the Amazonian Craton does not allow to compare our results with

specific potential sources. One lithic arenite (CE7) shows the older (Mesoarchean) Nd model age, which might have been imparted by lithic fragments coming from Archean sources. However, considering that the high $^{147}\text{Sm}/^{144}\text{Nd}$ ratio could have been caused by mafic contributions to the sediments, the model age may have been overestimated. A young (juvenile?) component is present in the microcrystalline (cherty) laminated quartz-rich layers that present a Sm-Nd model age of 1.81 Ga, which is very close to the depositional age (see below). The most likely potential sources with this age are the late-Orosirian sequences of the Rondonia-Juruena Province occurring to the south of the study region (Figs. 2 and 8B), which is in line with the detrital zircon data (significant age peak at 1.84 Ga). Older Paleoproterozoic (Siderian) and Archean sources were likely positioned to the east of Tapajós (e.g., Bacajá, Carajás, Rio Maria domains, basement of the Irixi-Xingu domain, and their counterparts in the Guyana Shield) (Fig. 8B).

7.2. Depositional age and tectonic setting

The Novo Progresso Formation was deposited in a NNW-SSE-trending graben, predominantly in alluvial and lake settings. The age of the youngest concordant detrital zircon (1836 ± 7 Ma) and the significant youngest peak (1846 Ma) set the maximum depositional age of the Novo Progresso Formation at about 1840 Ma (Fig. 8A), indicating

that this unit is not associated with the ca. 2000 Ma-old orogenic volcanic rocks of the Vila Riozinho Formation. Therefore, deposition occurred at the end of most of the anorogenic magmatic activity in the TGP, slightly after the onset of the intracontinental rift system (Uatumã SLIP), and before the development of the structurally discordant, grossly E-W- trending, Statherian continental basin (Crepori Basin, ~1780 Ma). Considering this timing relationship, the predominantly proximal sediment sources, and the lithological constitution of the formation, we interpret Novo Progresso as a basin associated with the evolution of the Uatumã SLIP (Fig. 9).

Acknowledgements

This paper is an outcome of the Metalogenia das Províncias Minerais do Brasil, area SE-Tapajós, undertaken by the Geological Survey of Brazil. The senior author thanks CNPq-Conselho Nacional de Desenvolvimento Científico e Tecnológico for a research grant (306798/2016-6). Reviews of Jean Michel Lafon and Moacir Macambira allowed us to improve the article and were greatly appreciated.

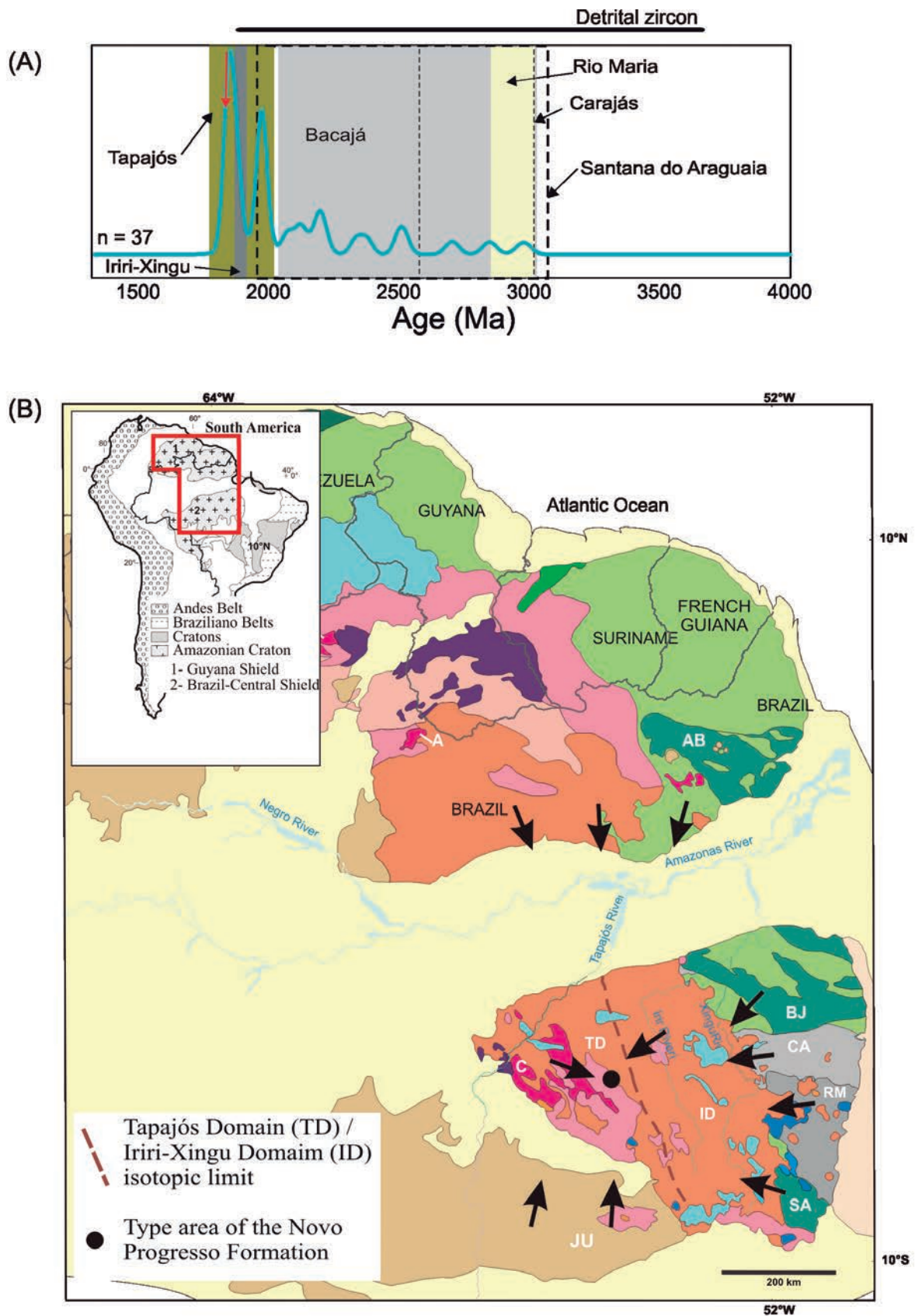


FIGURE 8 - (A) Probability density plot of detrital zircon ages for the Novo Progresso Formation displayed on the fields of ages of the magmatic events from tectonic domains of the central-southeastern portion of the Amazonian Craton. The upper thick bar shows the range of ages of detrital zircons from sedimentary basins within the same tectonic domains. Data compiled from Vasquez et al. (2008), Klein et al. (2012), Klein et al. (2014), Corrêa and Macambira (2014), Tavares (2015), and primary references in these works. (B) Simplified map of the Amazonian Craton with internal domains (modified from Fraga et al. 2017). Same legend as in Figure 1. The arrows show the potential source areas for the sediments of the Novo Progresso Formation.

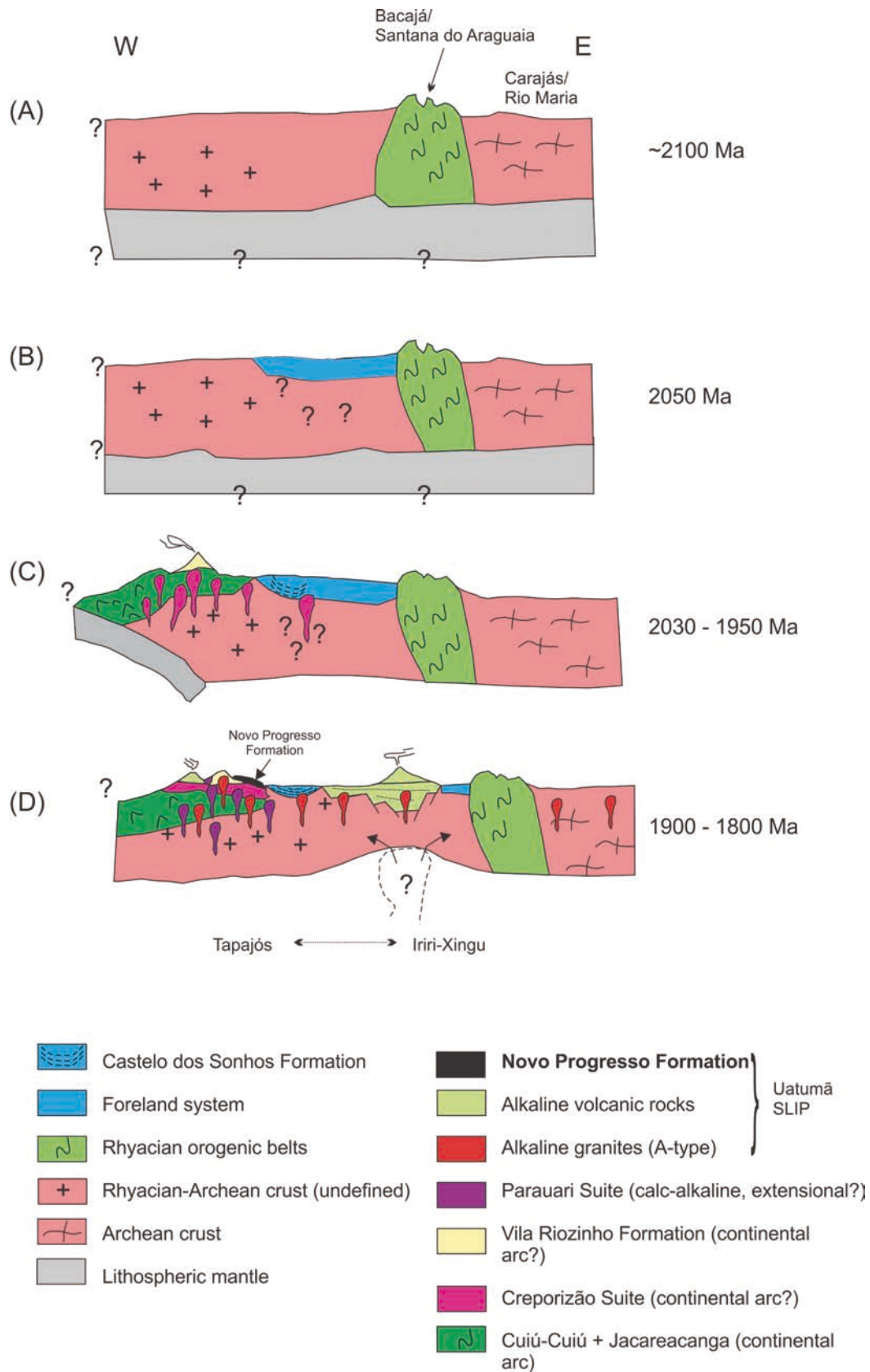


FIGURE 9 - Schematic (not to scale) W-E crustal sections of the SE Amazonian Craton depicting the proposed scenario for the geological evolution of the Novo Progresso Formation. Geological units are described in Figure 2 and the source areas (tectonic domains) are those presented in Figures 1 and 8. (A) Formation of Rhyacian orogenic belts. (B) Development of Rhyacian foreland systems over an Archean - Paleoproterozoic block. (C) Orogenic phase in the Tapajós Gold Province. (D) Extensional phase with intrusion of early granitoids followed by rifting and deposition of the Novo Progresso Formation (adapted from Klein et al. 2107). The Castelo dos Sonhos Formation was interpreted (Klein et al. 2017) as part of the foreland system, which remained in margin of the Tapajós domain after the Uatumã rifting.

References

- Andersen T., Andersson U.B., Graham S., Aberg G., Simonsen S.L. 2009. Granitic magmatism by melting of juvenile continental crust: new constraints on the source of Palaeoproterozoic granitoids in Fennoscandia from Hf isotopes in zircon. *Journal of the Geological Society*, 166, 233-247.
- Bühn B., Pimentel M.M., Matteini M., Dantas E.L. 2009. High spatial resolution analysis of Pb and U isotopes for geochronology by laser ablation multi-collector inductively coupled plasma mass spectrometry (LA-MC-ICP-MS). *Anais da Academia Brasileira de Ciências*, 81, 99-114.
- Chu N.C., Taylor R.N., Chavagnac V., Nesbitt R.W., Boella R.M., Milton J.A., German C.R., Bayon G., Burton K. 2002. Hf isotope ratio analysis using multi-collector inductively coupled plasma mass spectrometry: an evaluation of isobaric interference corrections. *Journal of Analytical Atomic Spectrometry*, 17, 1567-1574.
- Corrêa L.W.C., Macambira M.J.B. 2014. Evolução da região de Santana do Araguaia (PA) com base na geologia e geocronologia Pb-Pb em zircão de granitoides. *Geologia USP, Série Científica*, 14, 45-66.
- DePaolo D.J. 1988. Neodymium isotope geochemistry: An introduction. New York, Springer Verlag, 187 p.
- Ferreira A.L., Rizzotto G.J., Quadros M.L.E.S., Bahia R.B.C., Oliveira M.A. 2004. Folha SB.21-Tapajós. In: Schobbenhaus C., Gonçalves J.H., Santos J.O.S., Abram M.B., Leão Neto R., Matos G.M.M., Vidotti R.M., Ramos M.A.B., Jesus J.D.A. (eds.) Carta Geológica do Brasil ao Milionésimo, Sistemas de Informações Geográficas-SIG. Programa Geologia do Brasil, Brasília, CPRM, CD-ROM.
- Fraga L.M., Vasquez M.L., Almeida M.E., Dreher A.M., Reis N.J. 2017. A influência da orogenia Eo-Orosiriana na formação da SLIP Uatumã, parte central do Cráton Amazônico. In: Simpósio de Geologia da Amazônia, 15, 405-408.
- Gehrels G. 2012. Detrital zircon U-Pb geochronology: current methods and new opportunities. In: Busby C., Azor A. (eds.) *Tectonics of Sedimentary Basins: Recent Advances*, p. 47-62.
- Gioia S.M.L.C., Pimentel M.M. 2000. The Sm-Nd method in the geochronology laboratory of the University of Brasília. *Anais da Academia Brasileira de Ciências*, 72, 219-245.
- Griffin W.L., Pearson N.J., Belousova E., Jackson S.E., van Acherbergh E., O'Reilly S.Y., Shee S.R. 2000. The Hf isotope composition of cratonic mantle: LAM-MC-ICPMS analysis of zircon megacrysts in kimberlites. *Geochimica et Cosmochimica Acta*, 64, 133-147.
- Juliani C., Fernandes C.M.D., Monteiro L.V.S. 2015. Características da subducção, paleoclima e eventos erosivos paleoproterozoicos (2,1 - 1,88 Ga) e seus efeitos na estruturação da parte sul do Cráton Amazônico. In: Simpósio de Geologia da Amazônia, 13, SBG-NO, Annals (CD-ROM).
- Klein E.L., Almeida M.E., Rosa-Costa L.T. 2012. The 1.89-1.87 Ga Uatumã Silicic Large Igneous Province, northern South America. Large Igneous Provinces Commission. Available at: <<http://www.largeigneousprovinces.org>>.
- Klein E.L., Rosa-Costa L.T., Vasquez M.L. 2014. Metalogênese da borda oriental do Cráton Amazônico. In: Silva M.G., Rocha Neto M.B., Jost H., Kuyumjian R.M. (eds.) *Metalogênese das Províncias Tectônicas Brasileiras*. Belo Horizonte, CPRM, p. 171-194.
- Klein E.L., Rodrigues J.B., Queiroz J.D.S., Oliveira R.G., Guimarães S.B., Chaves C.L. 2017. Deposition and tectonic setting of the Palaeoproterozoic Castelo dos Sonhos metasedimentary formation, Tapajós Gold Province, Amazonian Craton, Brazil: age and isotopic constraints. *International Geology Review*, 59, 864-883.
- Lamarão C.N., Dall'Agnol R., Lafon J.M., Lima E.F. 2002. Geology, geochemistry and Pb-Pb zircon geochronology of the Paleoproterozoic magmatism of Vila Riozinho, Tapajós Gold Province Amazonian Craton, Brazil. *Precambrian Research*, 119, 189-223.
- Lamarão C.N., Dall'Agnol R., Pimentel M.M. 2005. Nd isotopic composition of Paleoproterozoic volcanic rocks of Vila Riozinho: implications for the crustal evolution of the Tapajós gold province, Amazon Craton. *Journal of South American Earth Sciences*, 18, 277-292.
- Ludwig K.R. 2003. *Isoplot 3.00 – A Geochronological Toolkit for Microsoft Excel*. Berkeley Geochronology Center, Special Publication, 4.
- Matteini M., Dantas E.L., Pimentel M.M., Bühn B. 2010. Combined U-Pb and Lu-Hf isotope analyses by laser ablation MC-ICP-MS: methodology and applications. *Annals of the Brazilian Academy of Sciences*, 82, 479-491.
- McLennan S.M., Hemming S., McDaniel D.K., Hanson G.N. 1993. Geochemical approaches to sedimentation, provenance, and tectonics. *Geological Society of America Special Paper*, 284, 21-40.
- Patchett P.J. 1983. Importance of the Lu-Hf isotopic system in studies of planetary chronology and chemical evolution. *Geochimica et Cosmochimica Acta*, 47, 81-97.
- Pettijohn F.J. 1975. *Sedimentary Rocks*. New York, Harper and Row.
- Queiroz J.D.S., Klein E.L., Rodrigues J.B. 2015. Rochas intrusivas na Formação Castelo dos Sonhos, Cráton Amazônico: petrografia, geocronologia, geoquímica e implicações para as idades de sedimentação e da mineralização no depósito aurífero Castelo de Sonhos. *Boletim do Museu Paraense Emílio Goeldi*, 10, 341-380.
- Santos J.O.S. 2003. Geotectônica do Escudo das Guianas e Brasil Central. In: Bizzi L.A., Schobbenhaus C., Vidotti R.M., Gonçalves J.H. (eds.) *Geologia, tectônica e recursos minerais do Brasil*. Brasília, CPRM - Serviço Geológico do Brasil, p. 169-226.
- Santos J.O.S., Groves D.I., Hartmann L.A., Moura M.A., Mcnaughton N.J. 2001. Gold deposits of the Tapajós and Alta Floresta Domains, Tapajós-Parima orogenic belt, Amazon Craton, Brazil. *Mineralium Deposita*, 36, 279-299.
- Santos J.O.S., Van Breemen O.T., Groves D.I., Hartmann L.A., Almeida M.E., Mcnaughton N.J., Fletcher I.R. 2004. Timing and evolution of multiple Paleoproterozoic magmatic arcs in the Tapajós Domain, Amazon Craton: constraints from SHRIMP and TIMS zircon, baddeleyite and titanite U-Pb geochronology. *Precambrian Research*, 131, 73-109.
- Semblano F.R.D., Pereira N.C.S., Vasquez M.L., Macambira M.J.B. 2016. Novos dados geológicos e isotópicos para o Domínio Iriri-Xingu, Província Amazônia Central; implicações para a idade do Grupo Iriri. *Revista USP, Série Científica*, 16, 19-38.
- Söderlund U., Patchett J.P., Vervoort J.D., Isachsen C.E. 2004. The ¹⁷⁶Lu decay constant determined by Lu-Hf and U-Pb isotope systematics of Precambrian mafic intrusions. *Earth and Planetary Science Letters*, 219, 311-324.
- Stern R.J. 2002. Crustal evolution in the East African orogen: A neodymium isotopic perspective. *Journal of African Earth Sciences*, 34, 109-117.
- Tassinari C.C.G., Macambira M.J.B. 2004. A evolução tectônica do Cráton Amazônico. In: Mantesso Neto V., Bartoreli A., Carneiro C.D.R., Brito-Neves B.B. (eds.) *Geologia do continente Sul-Americano: evolução da obra de Fernando Flávio Marques de Almeida*. São Paulo, Beca, p. 471-485.
- Tavares F.M. 2015. Evolução geotectônica do nordeste da Província Carajás. PhD Thesis, Instituto de geociências, Universidade Federal do Rio de Janeiro, Rio de Janeiro, 143 p.
- Vasquez M.L., Rosa-Costa L.T., Silva C.M.G., Klein E.L. 2008. Compartimentação tectônica. In: Vasquez M.L., Rosa-Costa L.T. (eds.) *Geologia e Recursos Minerais do Estado do Pará: Sistema de Informações Geográficas – SIG: texto explicativo dos mapas Geológico e Tectônico e de Recursos Minerais do Estado do Pará*. Escala 1:1.000.000. Belém, CPRM, p. 39-112.
- Vasquez M.L., Klein E.L., Ricci P.S.F. 2002. Granitoides pós-colisionais da porção leste da Província Tapajós. In: Klein E.L., Vasquez M.L., Rosa-Costa L.T. (eds.) *Contribuições à Geologia da Amazônia*, 3, 67-84.
- Vasquez M.L., Chaves C.L., Moura E.M., Oliveira J.K.M. 2017a. Programa Geologia do Brasil-PGB. Geologia e Recursos Minerais das folhas São Domingos, SA-21-Z-A-II e Jardim do Ouro, SA-21-Z-A-III, Estado do Pará, Escala 1:100.000. Belém, CPRM-Serviço Geológico do Brasil, 305 p.
- Vasquez M.L., Chaves C.L., Pinheiro F.G.R., Moura E.M., Castro J.M.R., Neto M.C.C., Cruz V.L. 2017b. Mapa de integração geológico-geofísica da ARIM Tapajós, Estado do Pará. Belém, CPRM, Escala 1:500.000 (available at <geosgb.cprm.gov.br>).